CONF-960850--8 ANL/ET/CP--88998

FABRICATION AND DESIGN OF A HIGH-CURRENT DOWNLINK USING Bi-BASED SUPERCONDUCTORS*

B. L. Fisher, M. T. Lanagan, and U. Balachandran
Energy Technology Division
Argonne National Laboratory
Argonne, IL 60439

S. Honjo and T. Hara
Tokyo Electric Power Company
Yokohama 230, Japan

August 1996

Paper to be presented at the 1996 Applied Superconductivity Conference, Pittsburgh, PA, August 25-30, 1996.

*Work supported in part by Tokyo Electric Power Company and in part by the U.S. Department of Energy (DOE), Energy Efficiency and Renewable Energy, as part of a DOE program to develop electric power technology, under Contract, W-31-109-Eng-38.

DISCLAIMER

Fabrication and Design of a High-Current Downlink Using Bi-Based Superconductors

B. L. Fisher, M. T. Lanagan, and U. Balachandran
Energy Technology Division
Argonne National Laboratory, Argonne, IL 60439–4838

S. Honjo and T. Hara
Tokyo Electric Power Company
Yokohama 230, Japan

Abstract— **Recent processing developments in $Bi_{1.8}Pb_{0.4}Sr_2Ca_2Cu_3O_x$ (BSCCO-2223) bars have produced bulk BSCCO-2223 bars with properties advantageous for power applications. Cold isostatically pressed (CIP) and sinter-forged BSCCO-2223 both have low AC loss, which make them desirable for use in power devices. Thermal conductivity of the CIP bars is lower than that of the previously used sinter-forged samples by a factor of 2. CIP bars with cross-sectional areas of ≈0.75 cm² and carrying 250 A RMS transport current have AC loss values of 30 μJ/cycle-cm at 50 Hz and 77 K. A pair of prototype downlinks were designed and built with sinter forged bars to deliver a continuous AC current of 1500 A over a temperature gradient of 77 to 4.2 K while delivering about ≈200 mW of heat to the liquid-helium-cooled end. This paper will discuss the design considerations and modeling of downlinks, which supply high AC currents over the 77 to 4.2 K temperature gradient with low thermal losses.**

I. Introduction

The low thermal conductivity and Joule heating of the HTS material compared to those of metallic conductors makes their use beneficial in reducing the cooling costs of current leads [1]. Many variables are associated with the design of a power downlink assembly, including HTS material type, assembly length, temperature gradient spanned, HTS lead geometry, total AC transport requirements, and cooling method. The various types of HTS conductors available include powder-in-tube (PIT) wire and bulk HTS. The PIT wire has a higher thermal conductivity than that of bulk HTS because of the Ag sheath. Silver can be doped to reduce thermal losses [2]; however, thermal losses are still greater than those of bulk bars [3],[4]. Potential cooling methods include conduction and convection cooling. Conduction cooling assumes that there is no additional cooling from gaseous vapors. Convection cooling assumes that the gaseous vapor is allowed to flow in intimate contact with the HTS bars and carry away heat. Applications will likely include both of these cooling methods. The present design uses a liquid nitrogen (LN_2) reservoir at the upper end, fixing the temperature at 77 K. The lower end of the downlink extends into a liquid helium (LHe) bath. The heat from conduction, ohmic and AC losses causes the LHe to boil; therefore, the gaseous vapor passes near the HTS bars and cools them.

II. Experimental Methods

A. Bar Fabrication and Processing

The bars used in this study are Pb-doped BSCCO-2223. The cold-isostatic-pressed (CIPed) bars are sinter-forged (hot-pressed) in order to bond a silver foil to the superconductor; the silver provides a low-resistance contact for current-lead attachment [5]. The CIPed bars are sinter-forged at 3 Pa for 1 hr at 820°C. These sinter-forged contact-pressed (SFCP) bars have a thermal conductivity that is ≈50% that of earlier full-sinter-forged (FSF) bars. The FSF bars were processed at 7 MPa for 4 hr at 840°C. In addition to thermal and electrical properties, mechanical properties are also important [6]-[8].

B. AC Loss Measurements

The AC loss is measured with an HP 8116A function generator, Kepco 20A/20V bipolar amplifier, transformer, calibrated noninductive resistor, and a Stanford Research SR830 DSP lock-in amplifier. The function generator, coupled with the bipolar amplifier, provides a sine wave of the desired amplitude and frequency. The current in the transformer secondary (I_2) is measured with the calibrated noninductive resistor. The voltage signal from the resistor (V_r) is measured with the lock-in amplifier, which shifts the internal reference phase until it matches the phase of the input signal V_r. The lock-in displays RMS magnitude of V_r, the lock-in phase with respect to the internal reference (now zero degrees), and the phase with respect to the external trigger reference (the phase of I_2). Then the voltage drop across the superconductor, V_s, is measured by the lock-in amplifier. The lock-in displays the RMS amplitude of V_s in phase with I_2 (the resistive component). The AC power loss per (Q) unit length is calculated by

$$Q = \frac{(I_2 \cdot V_s)}{(frequency \cdot e_{gap})} \qquad (1)$$

In (1), I_2 is the RMS magnitude of the transport current, V_s is the RMS magnitude of the resistive component of the voltage drop across the sample, and e_{gap} is the distance between the voltage taps [9]. Fig. 1 shows a schematic diagram of the AC loss apparatus. The DC transport current (I_c) was also measured at the same time.

Recent publications have brought up the question of the proper voltage lead geometry for making AC loss measurements [10]. These publications have shown that the voltage lead geometry is very important for superconductors with large aspect ratios (ratio of width to thickness), such as those found in PIT tapes. The AC loss was measured for several voltage lead configurations to determine if there is a dependence on the voltage lead distance, d, prior to twisting [11]. Fig. 2 shows that the AC loss values vary slightly as a function of d for low currents. However, in the current, I_{rms}, range of interest ($Q \geq 20$ μJ/cycle-cm) for lead applications, the AC loss data is identical for all test values of d. All presented AC loss data used $d \approx 0$.

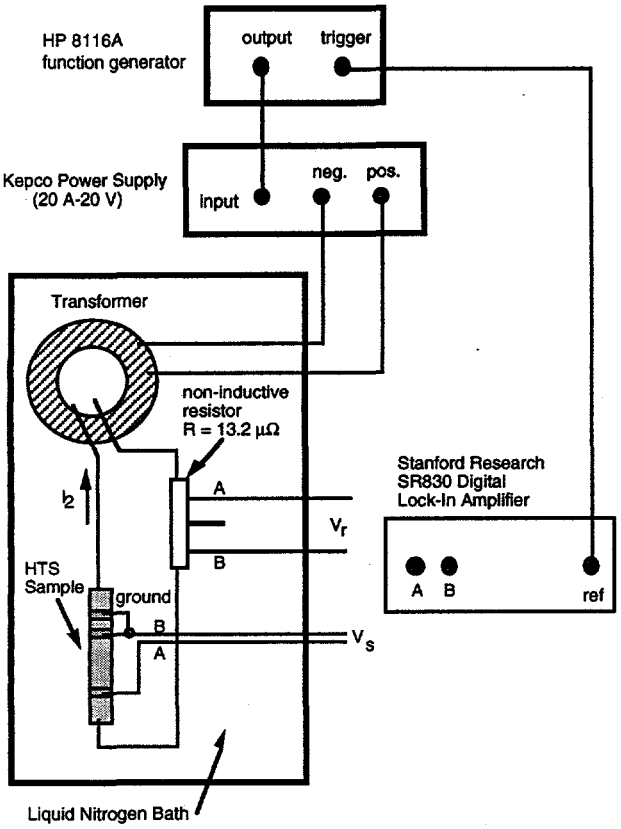

Fig. 1. Schematic diagram of AC loss apparatus.

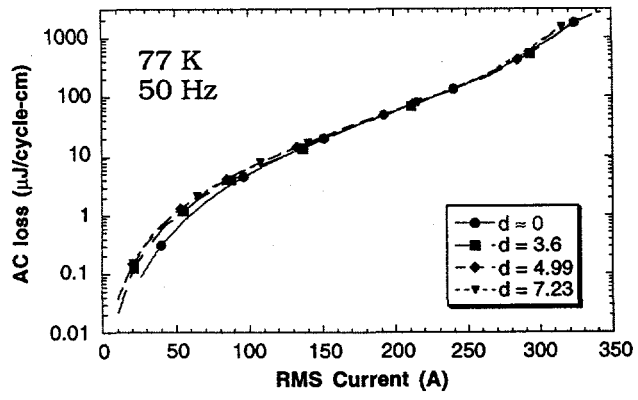

Fig. 2. Plot of AC loss vs. RMS current for several values of d.

C. Model Calculations

Many variables are involved in modeling the total heat delivered to the LHe. Total heat includes calculation of thermal, AC, and ohmic losses. The following thermal loss calculation assumes no convection cooling and no current flow.

$$Q_T = \frac{A}{l}\int_{4.2}^{77} k(T)dT. \qquad (2)$$

In (2) Q_T is the thermal heat delivered to the LHe, A is the cross-sectional area, l is the length of the sample, and k(T) is the thermal conductivity as a function of temperature [12]. The integrals of thermal conductivity were calculated to be 1.076 and 1.807 W/cm for the SFCP bars and FSF bars, respectively. This calculation is a conservative estimate of the thermal losses, because in our case, convective cooling from the He gas reduces the thermal loss and changes the temperature profile of the bar. This change in temperature profile will cause a larger portion of the bar to be cooler; it also affects AC loss, which is temperature-dependent.

The temperature profile of the bar is calculated from k(T) and the sample dimensions, based on the calculated thermal loss value. This profile is used to calculate total AC loss, which is temperature-dependent. The AC loss as a function of current was measured at both 77 and 4.2 K. Tests of bar samples at 4.2 K showed AC losses of only 0.05-0.25 of losses at 77 K (>0.10 at the desired operating current). The model assumes a linear fit of the AC loss over the temperature span from 77 to 4.2 K. Using the calculated temperature profile of the HTS bar, we calculated AC loss for discrete segments along the bar's length. The sum of the AC loss over the entire length is then calculated. This is again a conservative estimate of the losses, because the heat generated by the AC loss will replace a portion of the thermal heat needed to establish the thermal gradient.

In addition to the bar's thermal and AC losses, ohmic losses are caused by the contacts and additional AC losses (from the low temperature superconductor used to connect the downlink pair). The model assumes this ohmic contribution for the LHe cooled end only; the LN_2 heat sink should remove the heat contribution from the contacts at the upper end. The sinter-forging and contact-pressing provide low resistance contacts ≈ 20 nΩ at 4.2 K. Additional AC losses come from the low temperature superconductor (in our case NbTi) used to connect the pair of downlinks. There are no thermal-conductive-loss components associated with this link.

III. Results and Discussion

The AC loss and I_c of SFCP bars were studied as a function of the cross-sectional area (XSA). The XSA, I_c, and AC loss were measured for each sample. The XSA of the bar was then reduced by sanding, the contacts were reapplied by sinter-forging, and the bar was retested for I_c and AC loss.

Fig. 3, a graph of AC loss (Q) versus RMS current, shows a range of XSA values within which varying the XSA does not greatly change the operating current (I_{rms}) or AC loss. However, a change in the XSA does result in a significant change in thermal heat loss.

The data in Table I show that as a function of XSA, I_c decreases at a faster rate than the operating current (I_{rms}), for a given AC loss value (30 μJ/cycle-cm). Also, the J_c remains constant, taking into account self-field effects. The AC loss can be calculated for small changes in XSA, with the following (3). The equation, derived from [9], assumes that the losses are caused by magnetic hysteresis.

$$Q_{new} = \frac{XSA_{old}}{XSA_{new}} \cdot Q_{old}, \text{ for a given } I_{rms}. \quad (3)$$

The calculation agrees well with the data (see Table I), implying that the dominant effect is caused by magnetization hysteresis [9]. The data also show that for smaller XSAs, the bars can operate at higher current ratios, I_{rms}/I_c, while dissipating the same AC loss. The DC transport properties are dependent on XSA, because of self-field effects; however, the dependence of AC loss on XSA is much greater [13].

Fig. 4 is a plot of the calculated power loss versus bar length for various cross-sectional areas. The calculation assumes no gaseous He cooling and that all of the AC loss heat produced is delivered to the LHe. The third trace represents the middle XSA sample at the same current level (I_{rms}) as in the large XSA sample. Because thermal and AC losses are competing effects, thermal losses decrease with length and AC losses increase with length. Therefore, there is an optimal length for a given XSA to achieve the lowest total loss. However, when designing a downlink, there are overall current requirements, and bar-fabrication limitations must be considered.

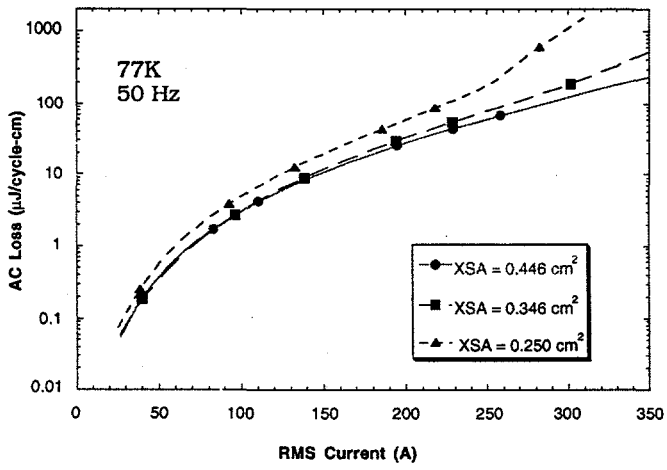

Fig. 3. Plot of AC loss vs. RMS current at 77 K and 50 Hz.

Table I
Electrical properties for several XSA values.

XSA (cm^2)	I_{rms} (A)	Q (μJ/cycle-cm) at 77 K	I_c (A)	J_c (A/cm^2)
0.446	205	30.0	469	1051
0.346	195	30.0	383	1107
0.346	205	37.4	383	1107
0.250	170	30.0	297	1188

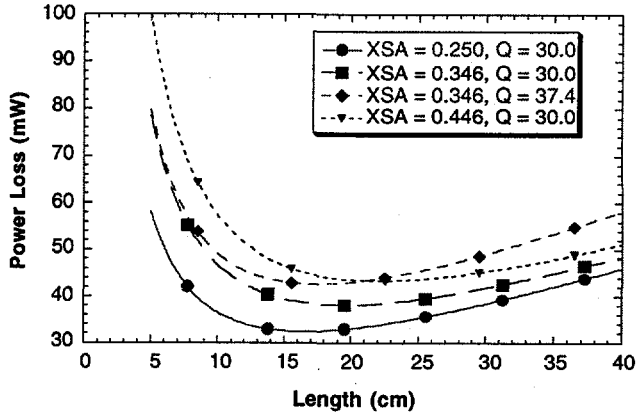

Fig. 4. Plot of power loss vs. length. Q is the AC loss at I_{rms}, 77 K, and 50 Hz. (see Table I).

Fig. 5 shows one of the prototype downlinks. The downlink was designed to carry 2000 A RMS with low thermal energy delivered to the LHe. Each downlink used six 7-in.-long SFCP bars.

IV. Conclusions

The total power loss of an AC downlink has many variables. The data show that significant reductions in thermal loss can be achieved by reducing the bar's cross-sectional area (XSA), while not greatly increasing the bar's AC loss. The above model (see Fig. 4) is a worst-case scenario for the power delivered to the LHe. In typical power applications, gaseous He is allowed to cool the assembly and this changes the temperature profile, resulting in lower AC and thermal losses. Therefore, the model calculates a higher power loss than would be measured in an He boiloff test. The model is useful in determining the optimal bar length to be used in HTS AC power downlinks.

Future work includes a study that will attempt to determine if the geometrical effect is caused entirely by the self field dependence or in part by the bar inhomogeneity. For example, Pb loss from the bar will alter the phase assemblage and degrade electrical properties at the bar surface. The proximity effects for various bar configurations will also be investigated. Further optimization of material composition will achieve higher I_{rms} values with reduced AC loss. Further attempts will also be made to improve contact technology.

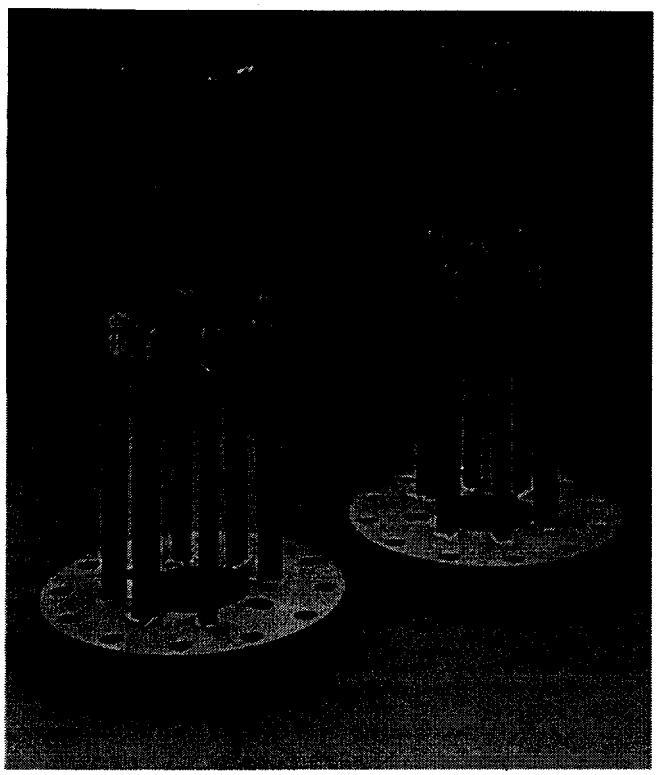

Fig 5. Prototype 2000-A RMS AC downlink. The downlink is shown inverted; the wires are NbTi and are used to connect the downlink.

ACKNOWLEDGMENT

We are grateful to Dr. Ctirad Uher of University of Michigan Dept. of Physics for the thermal conductivity measurements and to James Giumarra for participation in the AC loss measurements. Work supported in part by Tokyo Electric Power Company and in part by the U.S. Department of Energy (DOE), Energy Efficiency and Renewable Energy, as part of a DOE program to develop electric power technology, under Contract W–31–109–Eng–38.

REFERENCES

[1] J. R. Hull, "High-temperature superconducting current leads for cryogenic apparatus," *Cryogenics*, vol. 29, pp. 1116-1123, 1989.

[2] K. H. Sanhage, G. N. Riley, and W. L. Carter, "Critical issues in the OPIT processing of high-J_c BSCCO superconductors," *JOM*, vol. 43, pp. 21, 1991.

[3] C. Uher, *J. Supercond.*, vol. 3, 4, pp. 337-389, 1990.

[4] C. Uher, report to Argonne National Laboratory, Dec. 14, 1995 (unpublished).

[5] Y. Fang, S. Danyluk, M. T. Lanagan, C. A. Youngdahl, X. Xu, and K. Numata, "Characterization of Ag/$Bi_2Sr_2Ca_{n-1}Cu_nO_{2n+4}$ interfacial resistivity," *Physica C*, vol. 252, pp. 389-396, 1995.

[6] L. J. Martin, et al., "Mechanical properties of BiSrCaCuO/Ag superconductors," *Mater. Lett.*, vol. 17, pp. 232-236, 1993.

[7] S. E. Dorris, B. C. Prorok, M. T. Lanagan, S. Sinha, and R. B. Poeppel, "Synthesis of highly pure bismuth-2223 by two-powder process," *Physica C*, vol. 212, 66, 1993.

[8] K. C. Goretta, et al., "Processing and properties of bulk BiSrCaCuO superconductors," *Applied Supercond.*, vol. 2, 6, pp. 411-415, 1994.

[9] M. Basso, L. Lambardi, S. Marini, M. Marinelli, and A. Morpurgo, "Intergranular and intragranular current distribution in sintered YBCO from transport and inductive measurements," *Appl. Supercond.*, vol. 2, 2, pp. 71-91, 1994.

[10] M. Ciszek, A. M. Campbell, B. A. Glowacki, "The effect of potential contact position on AC loss measurements in superconducting BSCCO tape," *Physica C*, vol. 223, pp. 203-208, 1994.

[11] S. Fleshler, et al., "Measurement of the ac power loss of $(Bi,Pb)_2Sr_2Ca_2Cu_3)_X$ composite tapes," *Appl. Phys. Lett.*, vol. 6, 21, pp. 3189-3191, 1995.

[12] Y. Yamada, et al., "Superconducting current leads of Bi-based oxide," *IEEE Trans. Appl. Supercon.*, vol. 3, 1, pp. 923- 926, March 1993

[13] M. T. Lanagan, et al., "Effect of magnetic field on critical current density in bulk superconducting wires," *Proc. Mat. Res. Soc.*, vol. 169, 1996, pp. 1133-1135.